Experimental search for a 17-keV neutrino in the internal bremsstrahlung spectrum of ^{71}Ge

Y.S. Lee, M. Kobayashi, T. Hukutome, T. Horiguchi, and H. Inoue
Department of Physics, Faculty of Science, Hiroshima University, Higashi-Hiroshima, 724, Japan
(Received 15 November 1994)

We have performed a search for a 17-keV neutrino in the internal bremsstrahlung spectrum accompanying the electron capture decay of ^{71}Ge by using an ultra-large-size HpGe detector. Special attention was paid to get the well-reproducing response function, the accurate peak-detection efficiency, and the appropriate counting condition in which the pileup effect can be almost negligible. All these made it possible to compare the experimental spectrum with the theoretical one without using any shape factor or smooth function. We excluded the possibility of the 17-keV neutrino with mixing fraction of (1.6±0.8)% obtained by Žlimen *et al.* Our upper limit for the mixing fraction of the 17-keV neutrino was estimated to be 0.6% at 95% confidence level with Q=232.65 $^{+0.34}_{-0.24}$ keV.

PACS number(s): 14.60.Pq, 23.40.Bw, 27.50.+e

I. INTRODUCTION

The search for a heavy neutrino has been the subject of experimental investigation ever since evidence of a 17-keV neutrino with mixing fraction of (2–3)% was first claimed from the measurement of the β spectrum of tritium by Simpson [1] in 1985. There are two kinds of experimental methods to search for a 17-keV neutrino: One is to measure the electron from β decay by using magnetic spectrometers [2–10]. The other is to measure the photon emitted as the internal bremsstrahlung accompanying the electron-capture (IBEC) decay by using Ge spectrometers [11–15]. Žlimen *et al.* [11] investigated the IBEC spectrum of ^{71}Ge and reported evidence of a 17.2 $^{+1.3}_{-1.1}$ keV neutrino with a mixing fraction of (1.6±0.8)% at a 95% confidence level. However, a recent negative result by DiGregorio *et al.* [14] indicates the upper limit of mixing fraction of 0.5% (95% C.L.) from IBEC measurements for the same decay. Thus there are some contradictions for both results, and the results are not conclusive yet.

Since the EC decay of ^{71}Ge is an allowed transition to the ground state of ^{71}Ga [16], the theoretical IBEC spectra for the allowed transition can be exactly calculated with well-established theories [17, 18]. An extended useful review associated with IBEC is presented by Bambynek *et al.* [19]. The ^{71}Ge source can be easily produced through thermal neutron irradiation with a nuclear reactor. The experimental IBEC spectrum thus can be measured with the Ge spectrometer with high precision. We carried out the identification experiment of the 17-keV neutrino in the IBEC spectrum of ^{71}Ge which was measured by Žlimen *et al.* [11] and by DiGregorio *et al.* [14].

One of the difficulties for this experiment is to attain a high precision in the analysis of the measured IBEC spectrum. In other words, the IBEC measurement must be performed in compromise with statistical uncertainty and the systematic one. For this purpose, the efficiency and the response function of the detector were carefully investigated. We compared the measured IBEC spectrum with the calculated IBEC spectrum which was only convoluted by using the detector response function and the detector efficiency. In the comparison, the smooth functions (or shape factors) which have been used in the previous investigations [11, 14] are not used, because they may introduce some ambiguities in the comparison of the convoluted IBEC spectrum with the measured one.

In this experiment, we especially took care of the influences of several experimental conditions: the choice of source-to-detector distance, the self-absorption of IBEC in the source or in the materials covering the source, the reduction of the background, the suppression of the pileup, and the subtraction of the background and impurity peaks.

II. EXPERIMENTAL PROCEDURE

The ^{71}Ge ($T_{1/2}$=11.7 d) source was produced with a ^{70}Ge (n,γ) ^{71}Ge reaction by irradiating the Ge crystal of natural abundance (99.9999% purity) with thermal neutrons. The Ge crystal of about 70 mg was irradiated for 72 h with a neutron flux of 1×10^{14} neutrons/cm^2 sec from the JRR-3 reactor at the Japan Atomic Energy Research Institute (JAERI), and the disintegration rate of ^{71}Ge was about 6.5 GBq just after the irradiation. During the irradiation, ^{77}Ge ($T_{1/2}$=11.3 h) is simultaneously produced by the ^{76}Ge (n,γ) ^{77}Ge reaction. The gamma rays from the β decay of ^{77}As ($T_{1/2}$=1.6 d), which is the decay product of ^{77}Ge, were observed as main impurity peaks. Some other nuclides having shorter half-lives soon decayed out after the irradiation. The irradiation time and the starting time of measurement were chosen so that the ^{77}As/^{71}Ge ratio becomes low.

The ^{71}Ge source was supported on cellulose tape with a thickness of 0.05 mg/cm^2 in order to reduce the gamma-ray self-absorption in the source and the absorption in the supporter. The absorption was calculated from the tables compiled by Debertin and Helmer [20]. The total

gamma-ray absorptions were estimated to be less than 0.4% in the energy range above 100 keV, and can be therefore neglected for the sources used in this experiment. The single gamma-ray sources for the determination of response function and the ^{75}Se source for the efficiency calibration were also produced by irradiation in the reactor at JAERI. These sources were also prepared with cellulose tape of the same thickness as the ^{71}Ge source.

The spectrometer system of this experiment consists of a large-size coaxial-type HPGe detector (294 cm^3) with ultralow background design, an ORTEC 672 amplifier with pileup rejection circuit, an 8192 channels analog-to-digital (AD) converter, and a multichannel analyzer. The full widths at half maximum (FWHM) of the system are 0.86 keV and 1.81 keV at 122-keV and 1332-keV gamma rays, respectively. In order to reduce the background, the Ge detector was shielded by lead blocks of thickness 100–150 mm. The inside of the shield was covered with copper plates of thickness 5.0 mm to absorb characteristic x rays emitted from the lead blocks. Room temperature was kept constant within 1° during the whole measurements. The distance between the source and the end cap of detector is reproducibly maintained by means of a special holder with spacers.

The features of our measurement are as follows. All IBEC measurements were performed by fixing the source-to-detector distance at 10 mm to attain high counting statistics and to decrease the influence of the background for a desired statistics. The disadvantages for short source-to-detector distance are the increase of random summing and the increase of uncertainty of the efficiency due to the coincidence-summing effect and small changes in the source-to-detector distance. The effect is discussed later. We chose the shaping time constant of 2 μsec to reduce the pileup effect. The amplifier gain was adjusted so that the FWHM is more than 11 channels between 60 and 500 keV; i.e., the amplifier gain was about 0.114 keV per channel. The measurements were performed considering all of the above items and a check of the system was carried out daily. Each measurement of the ^{71}Ge spectrum was performed during 80 000 sec in live-time mode. The background spectrum was also measured during the same time repeatedly. Both measurements were recorded in separate files every day and repeated 45 times. However, the ^{71}Ge spectra having a counting rate of more than 1500 sec^{-1} were not used for the spectrum analysis to reduce the uncertainty due to the pileup. Consequently, the total accumulation time of raw ^{71}Ge spectra available amounted to 38 $\times$ 80 000 sec. The average counting rate in these ^{71}Ge spectra was approximately 600 sec^{-1}, and the dead time was less than 0.7%. The 38 spectra were added after the gain drifts were corrected. The background spectra were also added for 38 $\times$ 80 000 sec after the gain drift correction.

Peak position and FWHM were analyzed in each run. The drifts were less than two channels in all IBEC measurements. The energy calibration was performed by using the gamma-ray energies of ^{75}Se and ^{133}Ba which were determined with high precision by Kumahora [21]. As a result, the accuracy of the energy calibration was estimated to be about 5 eV in the regions from 66 to 400 keV. The total raw ^{71}Ge spectrum with impurity peaks and background is shown in Fig. 1. The background spectrum and the estimated pileup contribution are also shown in Fig. 1.

In order to determine the response function, especially the dependences of the FWHM of the peak and the tail-to-peak ratio on the gamma-ray energy, single gamma-ray spectra of ^{141}Ce (145 keV), ^{114m}In (190 keV), ^{51}Cr (320 keV), and ^{198}Au (412 keV) were measured at various source-to-detector distances. The detector efficiency in our experiment was determined by using a ^{75}Se source, because ^{75}Se emits many gamma rays of well-known photon-emission rates with an uncertainty of less than 1% in the region from 66 to 400 keV. The absolute source strength of ^{75}Se was determined by comparing it with a ^{133}Ba intensity standard source which was prepared at the Electrotechnical Laboratory in Japan. The absolute disintegration rate of the ^{133}Ba source was determined with an accuracy better than 0.5% by means of the 4π-γ coincidence method. The gamma-ray intensities per decay of ^{75}Se and ^{133}Ba have been determined with uncertainties less than 1% by Yoshizawa *et al.* [22].

Since the emission rate of IBEC of ^{71}Ge is intrinsically low, the source is desired to be put as close as possible to the detector so as to increase counting rate of the IBEC spectrum. But a short source-to-detector distance makes it difficult to determine the efficiency with high accuracy. In other words, the coincidence-summing effect increases with decreasing source-to-detector distance. Because of this effect, the detector efficiency cannot be determined with the same accuracy as attained for the far geometry without a coincidence-summing correction. The determinations of the efficiency with this correction have been studied by several groups [23–29]. They are only per-

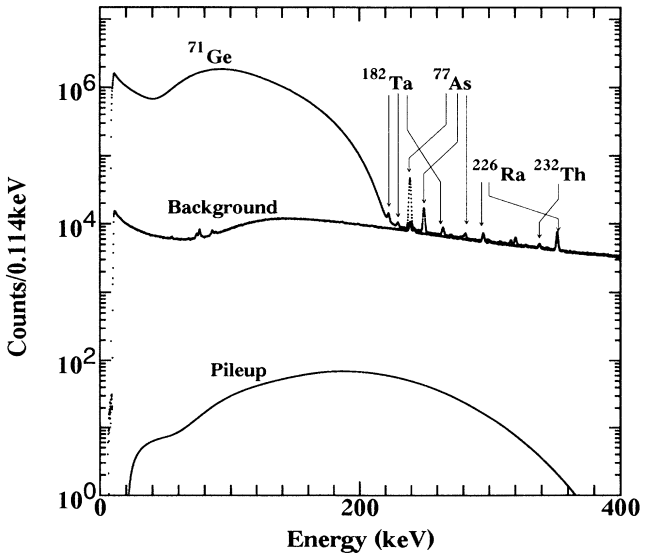

FIG. 1. The total raw IBEC spectrum of ^{71}Ge and the total background and pileup spectra.

formed at relatively large source-to-detector distances. Hence these methods cannot be applied to short source-to-detector distance as in this experiment. In order to attain the high-precision determination of efficiency, a method for the coincidence-summing correction was investigated [30]. In this method, the precision of the correction can be estimated by measurements at source-to-detector distances of 0, 10, 30, 50, 100, 150, and 200 mm between the source and the end cap of detector. In particular, the measurement of the efficiency at a 10-mm distance was repeated 5 times. The accuracy of the correction is estimated by checking the systematic variation of the efficiency after the coincidence-summing correction at the above distance.

III. DATA REDUCTION

In order to obtain a net IBEC spectrum of ^{71}Ge, the background, impurities, and pileup contributions are subtracted from the total raw ^{71}Ge spectrum. The procedures are to be described in detail as below.

A. Background and impurity subtractions

Most of the peaks in the background and measured ^{71}Ge spectra were identified as belonging to Ra and Th decay chains. The remaining impurity peaks were due to gamma rays of ^{77}As and ^{182}Ta as a contamination in the Ge source. Since the background spectrum was repeatedly measured for equal time with the ^{71}Ge spectrum, the added total background spectrum was subtracted, after the gain drift correction, from the total raw ^{71}Ge spectrum without any normalization.

In order to subtract the remaining impurity peaks from the background-subtracted ^{71}Ge spectrum, we prepared two independent impurity spectra. One is the ^{77}As spectrum which was prepared using the ^{71}Ge spectrum with strong peaks of ^{77}As at the earliest stage of the IBEC measurement. The other is the ^{182}Ta standard-source spectrum measured separately. For the spectrum normalization, the peak areas were determined by Gaussian fitting. The ^{77}As spectrum was normalized by the peak areas of the 236-keV gamma ray of ^{77}As and subtracted from the background-subtracted ^{71}Ge spectrum. With a similar procedure, the impurity peaks of ^{182}Ta were subtracted after being normalized by the peak areas of the 222-keV gamma ray of ^{182}Ta.

B. Pileup subtraction

The pileup effect depends on the counting rate. The distortion of the spectrum due to the pileup increases with increasing counting rate. Several methods of the pileup correction for full-energy peaks are proposed [31–37]. In particular, the problems of the correction method using a pulser were pointed out by Debertin and Schötzig [37]. However, no appropriate method has been proposed for the correction of a continuous spectrum like the IBEC spectrum.

In our experiment, the contribution of the pileup could be estimated from the ^{71}Ge spectrum itself in which the distortion due to pileup can be assumed to be sufficiently small. The normalized counting rate P_i in each channel was obtained for the ^{71}Ge spectrum with a low counting rate (~ 250 sec^{-1}) by

$$P_i = \frac{n_i}{N_t}, \tag{1}$$

where n_i is the count in channel number i and N_t is the total count recorded in the whole spectrum. Hence, the contribution can be obtained by convoluting the counting rates P_i with the assumption that any two pulses, which were too close in time to be sufficiently rejected by the pileup rejection circuit, combine to yield the sum pulse with height equal to approximately the sum of the heights of two pulses between the threshold k_1 (≈ 85 channel) and the end point k_2 (≈ 1950 channel) of the IBEC spectrum. Therefore, the shape of the contribution P_k, as a function of the sum of heights of two pulses, is given by

$$P_k = N \sum_{j=k_1}^{k_2} P_j P_{k-j} \quad (k = 2k_1\text{–}2k_2), \tag{2}$$

where N is a factor to represent the amount of the pileup contribution to the net ^{71}Ge spectrum.

The resulting pileup contribution was fitted to the net ^{71}Ge spectrum in the region above the end point, and was subtracted. The pileup contribution is also shown in Fig. 1 and was estimated to be less than 0.15% in the energy range near 205 keV. Indeed, as can be seen in Fig. 1, the difference between the total raw ^{71}Ge spectrum and the background spectrum is much smaller than previous studies [11, 14] in the region above the end-point energy. The pileup effect in our experiment is almost negligible in comparison with the statistical fluctuations of the net ^{71}Ge spectrum within one standard deviation.

C. Response function

In order to generate a response function at a given energy, we investigated the energy dependence of the tail-to-peak ratio and FWHM of the peaks using single gamma-ray sources of ^{141}Ce, ^{114}In^{m}, ^{51}Cr, and ^{198}Au. The typical spectra of these sources are shown in Fig. 2. The dashed lines indicate a base line of *zero*. As shown in Fig. 2, each spectrum has very small tail-to-peak and Compton-to-peak ratios. To investigate the details of the full-energy-peak regions, enlarged spectra of the regions are shown in Fig. 3 for ^{114}In^{m} and ^{198}Au. It is found that the tail-to-peak ratios depend on the gamma-ray energy; i.e., the ratio increases with the decrease of energy. In particular, as shown in Fig. 3, it is interesting to note that the peak has a low-energy bump that shows a deviation from the Gaussian shape, and also has a flat tail in the lower-energy side. This flat tail is found to be almost constant over the region of 30 keV (more than approximately 300 channels).

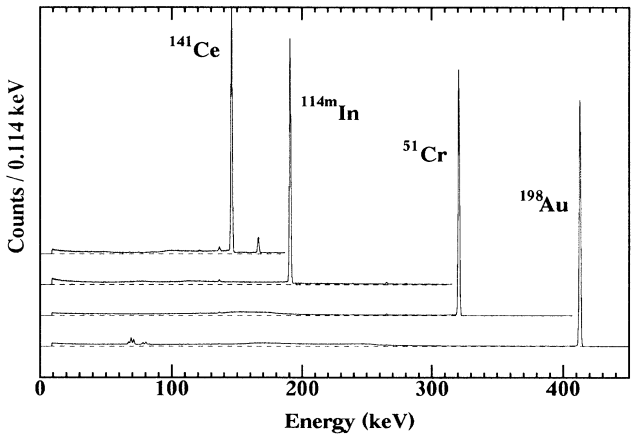

FIG. 2. Typical single gamma-ray spectra of ^{141}Ce, ^{114}In^{m}, ^{51}Cr, and ^{198}Au. Each spectrum was normalized with the height of the full-energy peak. The dashed lines mean a base line of *zero*.

In the present study, we compare the experimental and the theoretical IBEC spectra in the narrow energy range of 190–220 keV which covers the expected kink position due to a heavy neutrino with 10–20 keV mass range. Therefore, concerning the response function, it is not necessary to be such a complex function as to represent whole spectral region including the Compton edge. On the contrary, it is preferred to be rather a simple form to avoid ambiguity. In consequence, the response function

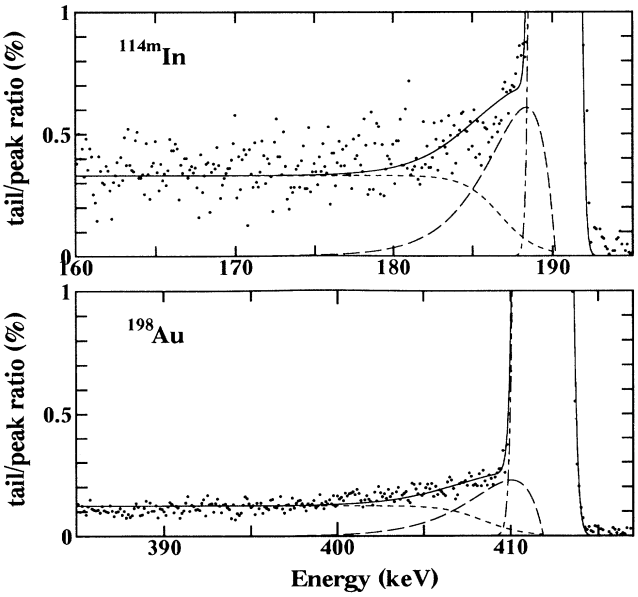

FIG. 3. Expanded spectra of ^{114}In^{m} (190 keV) and ^{198}Au (412 keV) to show the details near the full-energy peak. Ordinates show the flat tail to full-energy peak ratios. The fitted response functions are also shown by the solid lines. Dot-dashed, dashed, and dotted lines correspond to Gaussian, modified exponential, and flat tail functions, respectively.

$F(E)$ as a function of energy E in keV was assumed to consist of the following three analytical functions:

$$F(E) = a_1 \exp\{-a_2(E_0 - E)^2\} + b_1(E_0 - E)\exp\{-b_2(E_0 - E)\} + \frac{c_1}{1 + c_2 \exp\{(E_0 - E)/c_3\}}, \quad (3)$$

where E_0 is the peak-center energy, and the parameters a, b, and c with suffix depend on the photon energy E_0. In Eq. (3), the first term is a Gaussian function to represent the full-energy peak, and the next term is a modified exponential function defined for $E < E_0$ to represent the low-energy bump just below the Gaussian. The final term is a function to represent the continuous flat tail.

The resulting response functions fitted with Eq. (3) are shown in Fig. 3 for the spectra of ^{114m}In (190 keV) and ^{198}Au (412 keV) after the background subtraction. In Fig. 3, each term of Eq. (3) is represented with dot-dashed, dashed, and dotted lines. The solid curve represents the response function including the above three terms. It is clear that the experimental spectra are well reproduced by Eq. (3).

The energy dependences of the tail-to-peak ratio $r(E_0)$ and FWHM $fw(E_0)$ in keV were found to be represented with the following forms as a function of photon energy E_0:

$$r(E_0) = A_1 + A_2 E_0, \quad (4)$$

$$fw^2(E_0) = B_1 + B_2 E_0, \quad (5)$$

where the parameter values were determined to be $A_1 = (5.41 \pm 0.52) \times 10^{-3}$, $A_2 = (-9.89 \pm 0.15) \times 10^{-6}$, $B_1 = 1.165 \pm 0.101$, and $B_2 = (1.474 \pm 0.020) \times 10^{-3}$ by the least-squares method. The ratios and FWHM in the energy range 145–412 keV were estimated to be approximately (0.13–0.4)% and 1.17–1.33 keV, respectively. The resulting response function is satisfactory enough for the search for a heavy neutrino in the localized energy region in this study.

D. Efficiency

The peak-detection efficiency of the HPGe detector was determined by using ^{75}Se standard source with the following procedure. First, the linear background under the peak was subtracted from each peak of the ^{75}Se spectrum, and then the peak area was determined by a Gaussian fitting. The apparent efficiencies were obtained from the peak areas and the gamma-ray intensities per decay of ^{75}Se, and the values are shown in Fig. 4 with open circles for several source-to-detector distances from 0 to 200 mm. As shown in the figure, the efficiencies decrease smoothly with the increase of energy in the region above 136 keV for distances larger than 50 mm. However, it can be seen that the value for the 401-keV gamma ray becomes relatively large at distances below 30 mm. This is caused by the coincidence-summing effect.

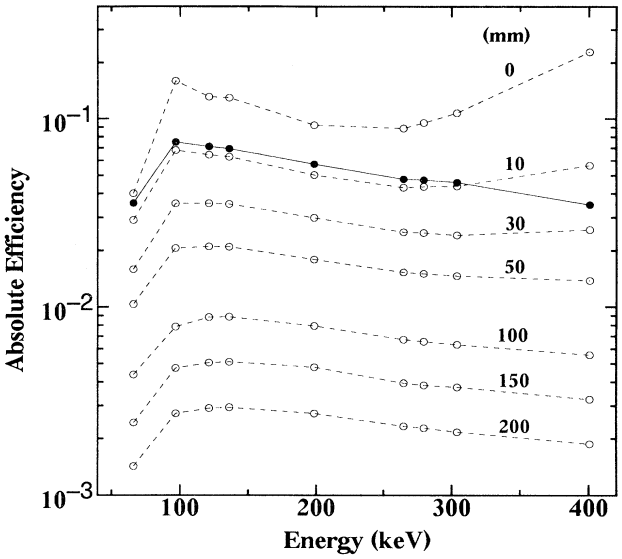

FIG. 4. The open circles show the apparent peak-detection efficiencies for several source-to-detector distances from 0 to 200 mm. The solid circles are the corrected ones for the coincidence-summing effect at a 10-mm distance.

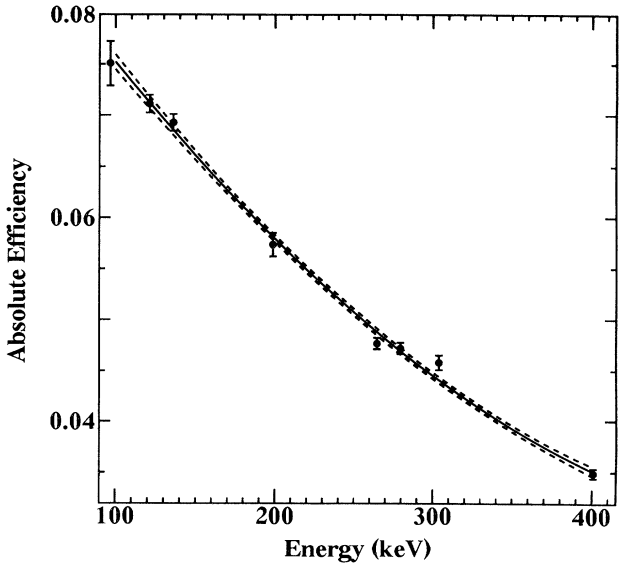

FIG. 5. Solid circles with error bars represent the corrected efficiencies at a 10-mm source-to-detector distance. The solid curve indicates the best-fitted efficiency curve in the region between 100 and 400 keV. The dashed lines indicate the uncertainty of the efficiency curve within one standard deviation.

Therefore, we tried to correct the coincidence-summing effect considering the decay scheme of ^{75}Se. A detailed description for the correction method will be described elsewhere [30]. As a result, the efficiencies at a 0-mm distance were found to still have distortion even after the coincidence-summing correction. The corrected efficiencies at a 10-mm distance are also represented in Fig. 4 with solid circles. As can be seen in the figure, the effect was corrected almost completely and the relative uncertainties were less than 1.4% in the region between 100 and 400 keV.

In order to determine the efficiency curve for the source-to-detector distance of 10 mm in the region from 100 to 400 keV, we tried to fit the corrected efficiencies with polynomials of order 1–3 and an exponential function. The value for the 66-keV gamma ray is far from the region of interest and was excluded from the fit. As a result of the fit, it was found that there is no significant difference between the quadratic polynomial function and the exponential function. Therefore, we finally adopted the quadratic polynomial function for the efficiency curve $\varepsilon(E)$ in the region 100–400 keV at a 10-mm distance:

$$\varepsilon(E) = a + bE + cE^2, \tag{6}$$

where E is the photon energy in keV, and a, b, and c are fitting parameters. The values were found to be $a=(9.645\pm0.186)\times10^{-2}$, $b=(-2.322\pm0.146)\times10^{-4}$, and $c=(1.966\pm0.268)\times10^{-7}$.

The uncertainty of the efficiency curve $\varepsilon(E)$ consists of the following components: (1) statistical uncertainties of peak areas, (2) systematic uncertainties from intensities per decay of ^{75}Se, (3) systematic uncertainties from coincidence-summing correction, and (4) the uncertainties deriving from the fitting of Eq. (6) including the correlation terms among a, b, and c. Hence, the uncertainty σ_ε of the efficiency curve ε is given by

$$\sigma_\varepsilon^2 = \sigma_a^2 + 2v_{ab}E + (\sigma_b^2 + 2v_{ac})E^2 + 2v_{bc}E^3 + \sigma_c^2E^4. \tag{7}$$

In Eq. (7), the correlation terms including $v_{ab}=-2.620\times10^{-8}$, $v_{ac}=4.531\times10^{-11}$, and $v_{bc}=-3.860\times10^{-13}$ have large contributions to σ_ε^2, and thus cannot be neglected in the uncertainty of the efficiency curve ε. The best-fitted efficiency curve of the quadratic polynomial is shown in Fig. 5, and the uncertainty of the efficiency curve is also represented within one standard deviation with dashed lines. The efficiencies near 200 keV are important for our present purpose.

IV. ANALYSES AND RESULTS

Since IBEC is a higher-order decay process in which an electron emits a photon with a probability of less than 10^{-4} per electron-capture event, IBEC shows a continuous spectrum, $dW(E)/dE$, as a function of photon energy E, like the usual β spectrum. By considering two kinds of neutrinos which are eigenstates with light mass m_L and heavy mass m_H, the IBEC spectrum becomes a sum of contributions from the neutrinos of both states: Thus we get

$$\frac{dW(E)}{dE} = \frac{dW(E,m_L)}{dE}\cos^2\theta + \frac{dW(E,m_H)}{dE}\sin^2\theta, \tag{8}$$

where $\sin^2\theta$ is the mixing fraction of a neutrino with mass m_H. Equation (8) is a general expression of the

IBEC spectrum for the emission of two neutrinos with masses m_L, which is assumed to be zero, and m_H. If m_H is assumed to be nonzero in Eq. (8), a kink will appear at the threshold energy for the emission of a heavy neutrino with mass m_H in the IBEC spectrum.

Typical IBEC spectra for the captures from a variety of electron orbits have the following forms: The expressions for the IBEC spectra from nS- and nP-state captures are given by

$$\frac{dW_{nS}(E,m_\nu)}{dE} \propto E\{Q-B(nS)-E\}\{[Q-B(nS)-E]^2 - m_\nu^2c^4\}^{\frac{1}{2}} R_{nS}(E), \quad (9)$$

$$\frac{dW_{nP_j}(E,m_\nu)}{dE} \propto E\{Q-B(nP_j)-E\}\{[Q-B(nP_j) - E]^2 - m_\nu^2c^4\}^{\frac{1}{2}} Q_{nP_j}^2(E), \quad (10)$$

where m_ν, Q, $B(nS)$, and $B(nP)$ are the mass of the neutrino, the transition energy, the binding energies of the S and P orbits, respectively. $R_{nS}(E)$ and $Q_{nP_j}(E)$ are correction factors which represent modifications for the Coulomb effect and the full relativistic effect. The suffixes n and j mean the major shell and subshell, respectively. Theoretical IBEC spectra for $1S$- and $2S$-state captures were calculated with Eq. (9) using the theory of Glauber and Martin [17], and the theoretical ones for $2P$- and $3P$-state captures were calculated with Eq. (10) using the theory of De Rújula [18].

The calculated IBEC spectrum was convoluted using the efficiency curve and the response function obtained in the previous section. The comparison between the convoluted IBEC spectrum and the net IBEC spectrum of ^{71}Ge was performed in 0.114 keV/channel bin by means of the χ^2 analysis. The steps of the χ^2 analysis are as follows: (1) the determination of the Q value for the EC decay of ^{71}Ge, which does not depend on the heavy neutrino, and (2) the determination of m_H and $\sin^2\theta$ from the spectra around the expected kink.

In the χ^2 analysis for step (1), the convoluted IBEC spectrum was fitted to the net IBEC spectrum of ^{71}Ge for ten different fitting regions in order to avoid arbitrariness in the choice of fitting regions. The Q value in the χ^2 analysis was varied in the range of 220–240 keV by steps of 0.01 keV, and the resulting best-fitted Q value was found to be 232.65 keV. The uncertainty associated with the χ^2 analysis was estimated to be $^{+0.16}_{-0.11}$ keV at a 68% confidence level. The systematic errors for the Q value are obtained from the following items: (a) the normalization factors for the subtractions of impurity peaks of ^{77}As and ^{182}Ta, (b) the normalization factor N in Eq. (2), and (c) the parameters in Eqs. (4), (5), and (6). To estimate the systematic errors, the normalization factors of items (a) and (b) were changed within ±30% and the consequent changes of the Q value were examined. As a result, the change due to item (a) caused the shift of the Q value by 0.03 keV, but the change due to item (b), i.e., the pileup contribution, was found to cause a negligibly small shift for the Q value. Next, the parameters of item (c) were changed within one standard deviation.

TABLE I. Comparison of the result of present experiment with the previous ones.

Authors	Q value (keV)	$\sin^2\theta$[a] (%)	Remarks
Bisi *et al.* [39]	231±3 (1σ)	-	IBEC
Wapstra and Audi [38]	235.7±1.8 (1σ)	-	Mass chain
Žlimen *et al.* [11]	$229.2^{+1.1}_{-0.9}$ (2σ)	1.6±0.8	IBEC
DiGregorio *et al.* [14]	232.1±0.1 (1σ)	< 0.5	IBEC
The present experiment	$232.65^{+0.34}_{-0.24}$ (2σ)	< 0.6	IBEC

[a]These values are cited with a 95% confidence level.

The consequent change of the Q value for the tail-to-peak ratio parameters in Eq. (4) was found to be 0.04 keV at a 68% confidence level, but the changes for ones in Eqs. (5) and (6) were very small and could be neglected. These systematic errors were thus added in quadrature to the uncertainty associated with the χ^2 analysis. As a result, the total error for the Q value was found to be $^{+0.17}_{-0.12}$ keV at a 68% confidence level.

The determined Q value is compared in Table I with those of previous studies. As shown in Table I, our Q value agrees with the Q value by Bisi *et al.* [39], but disagrees with the one compiled by Wapstra and Audi [38]. The Q value obtained by Žlimen *et al.* [11] is smaller than our value, but the one by DiGregorio *et al.* [14] is close to our value though the difference is beyond the errors. The

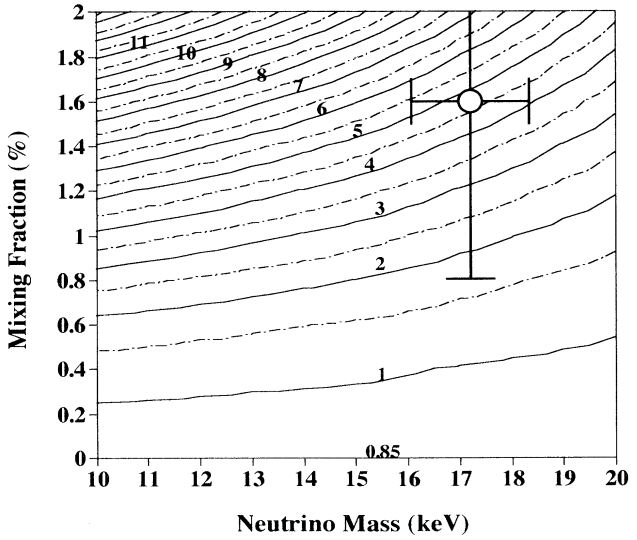

FIG. 6. The contour plot of the resulting χ^2_ν values as a function of the neutrino mass m_H and the mixing fraction $\sin^2\theta$. The circle with error bars indicates the result obtained by Žlimen *et al.* [11].

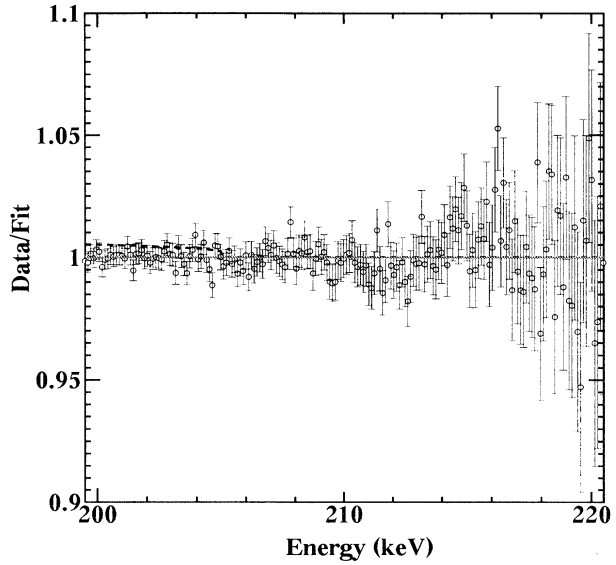

FIG. 7. Open circles show the ratios of experimental data to the best theoretical fit with m_H=17 keV and $\sin^2\theta$=0%. The dashed line corresponds to the ratio of the theoretical fit with $\sin^2\theta$=0.6% to the theoretical fit with $\sin^2\theta$=0% at m_H=17 keV.

discrepancies may be caused by the accuracy of the detector efficiency, the different shapes of response functions, and especially by the treatment of the shape factor (or smooth function) which is not used in this experiment.

The χ^2 analysis of step (2) to search for a heavy neutrino was limited in the 10–20 keV mass range, because the purpose of our experiment is to examine the possibility of the 17-keV neutrino emission in the IBEC spectrum of ^{71}Ge claimed by Žlimen *et al.* [11]. The χ^2 analysis with two free parameters m_H and $\sin^2\theta$ was intensively performed with 200 data points in the region where a kink is expected. The parameters m_H and $\sin^2\theta$ were independently varied by the steps of 1 keV and 0.05%, respectively, to get the minimum of the reduced chi square χ^2_ν.

The contour plot of the obtained χ^2_ν value is represented in Fig. 6 as a function of the neutrino mass m_H and the mixing fraction $\sin^2\theta$. In the figure, we could not find the local minimum anywhere on the (m_H, $\sin^2\theta$) plane. The circle with error bars indicates the result by Žlimen *et al.* [11]. As can be seen from Fig. 6, our χ^2_ν is about 1.7 for the point at m_H=17 keV and $\sin^2\theta$=0.8% which corresponds to the lower limit of the mixing fraction (1.6± 0.8)% obtained by Žlimen *et al.* This χ^2_ν value is twice larger than the χ^2_ν=0.85 at m_H=17 keV and $\sin^2\theta$=0% in Fig. 6. From the χ^2 test for the value of χ^2_ν=1.7 at m_H=17 keV and $\sin^2\theta$=0.8%, the possibility of the 17-keV neutrino can be excluded at a 99.9% confidence level in the present experiment. Moreover, the mixing fraction of the 17-keV neutrino was found to be less than 0.5% at a 95% confidence level from the present result. The change of $\sin^2\theta$ due to the uncertainty of our Q value, $^{+0.34}_{-0.24}$ keV at a 95% confidence level, was estimated to be less than 0.1%. Therefore, the upper limit of the mixing fraction of the 17-keV neutrino was estimated to be 0.6% at a 95% confidence level in the present experiment.

Figure 7 shows the ratio of the experimental spectrum to the theoretical one with $\sin^2\theta$=0%. Open circles in the figure show the ratios and the dashed line also shows the ratio of the theoretical spectrum with $\sin^2\theta$=0.6% to the theoretical one with $\sin^2\theta$=0% for m_H=17 keV. From this figure, it is obvious that there is no evidence for the 17-keV neutrino.

V. CONCLUSIONS

We have performed the search for the 17-keV neutrino in the IBEC spectrum of ^{71}Ge. Special consideration was taken to get the well-reproducing response function, the accurate peak-detection efficiency, and the appropriate counting condition in which the pileup effect can be almost negligible. All these made it possible to compare the experimental spectrum with the theoretical one without using any shape factor or smooth function.

In conclusion, we excluded the possibility of the 17-keV neutrino with mixing fraction (1.6±0.8)% obtained by Žlimen *et al.* [11] at a 99.9% confidence level. This result is in agreement with the result by DiGregorio *et al.* [14]. Our upper limit for the mixing fraction of the 17-keV neutrino was estimated to be 0.6% at a 95% confidence level with Q=232.65 $^{+0.34}_{-0.24}$ keV.

ACKNOWLEDGMENTS

The authors would like to express their sincere thanks to Prof. I. Endo, Hiroshima University, for his useful advice and encouragement. They also thank the staff of the Radioisotope center of Hiroshima University for allowing us use of the experimental facilities.

[1] J.J. Simpson, Phys. Rev. Lett. **54**, 1981 (1985).
[2] T. Altzitzoglou, F. Calaprice, M. Dewey, M. Lowry, L. Piilonen, J. Brorson, S. Hagen, and F. Loeser, Phys. Rev. Lett. **55**, 799 (1985).
[3] T. Ohi, M. Nakajima, H. Tamura, T. Matsuzaki, T. Yamazaki, O. Hashimoto, and R.S. Hayano, Phys. Lett. **160B**, 322 (1985).
[4] J. Markey and F. Boehm, Phys. Rev. C **32**, 2215 (1985).
[5] D.W. Hetherington, R.L. Graham, M.A. Lone, J.S. Geiger, and G.E. Lee-Whiting, Phys. Rev. C **36**, 1504 (1987).
[6] B. Sur, E.B. Norman, K.T. Lesko, M.M. Hindi, R.M. Larimer, P.N. Luke, W.L. Hansen, and E.E. Haller, Phys. Rev. Lett. **66**, 2444 (1991).

[7] M.Y. Bahran and G.R. Kalbfleisch, Phys. Lett. B **291**, 336 (1992).
[8] H. Kawakami, S. Kato, T. Ohshima, C. Rosenfeld, H. Sakamoto, T. Sato, S. Shibata, J. Shirai, Y. Sugaya, T. Suzuki, K. Takahashi, T. Tsukamoto, K. Ueno, K. Ukai, S. Wilson, and Y. Yonezawa, Phys. Lett. B **287**, 45 (1992).
[9] J.L. Mortara, I. Ahmad, K.P. Coulter, S.J. Freedman, B.K. Fujikawa, J.P. Greene, J.P. Schiffer, W.H. Trzaska, and A.R. Zeuli, Phys. Rev. Lett. **70**, 394 (1993).
[10] G.R. Kalbfleisch and M.Y. Bahran, Phys. Lett. B **303**, 355 (1993).
[11] I. Žlimen, A. Ljubičić, S. Kaučić, and B.A. Logan, Phys. Rev. Lett. **67**, 560 (1991).
[12] I. Žlimen, E. Browne, Y.D. Chan, M.T.F. da Cruz, A. Garcfa, R.M. Larimer, K.T. Lesko, E.B. Norman, R.G. Stoktad, and F.E. Wietfeldt, Phys. Rev. C **46**, 1136 (1992).
[13] F.E. Wietfeldt, Y.D. Chan, M.T.F. da Cruz, A. Garcia, R.M. Larimer, K.T. Lesko, E.B. Norman, R.G. Stokstad, and I. Žlimen, Phys. Rev. Lett. **70**, 1759 (1993).
[14] D.E. DiGregorio, S. Gil, H. Huck, E.R. Batista, A.M.J. Ferrero, and A.O. Gattone, Phys. Rev. C **47**, 2916 (1993).
[15] M.M. Hindi, R.L. Kozub, and S.J. Robinson, Phys. Rev. C **49**, 3289 (1994).
[16] E. Browne and R.B. Firestone, *Table of Radioactive Isotopes* (Wiley, New York, 1986).
[17] R.J. Glauber and P.C. Martin, Phys. Rev. **104**, 158 (1956); P.C. Martin and R.J. Glauber, Phys. Rev. **109**, 1307 (1958).
[18] A. De Rújula, Nucl. Phys. **B188**, 414 (1981).
[19] W. Bambynek, H. Behrens, M.H. Chen, B. Craseman, M.L. Fitzpatrick, K.W.D. Ledingham, H. Genz, M. Mutterer, and R.L. Intemann, Rev. Mod. Phys. **49**, 1 (1977).
[20] K. Debertin and R.G. Helmer, *Gamma- and X-ray Spectrometry with Semiconductor Detectors* (North-Holland, New York, 1988).
[21] H. Kumahora, Nucl. Instrum. Methods A **238**, 431 (1985).
[22] Y. Yoshizawa, Y. Iwata, T. Katoh, J.Z. Ruan, and Y. Kawada, Nucl. Instrum. Methods **212**, 249 (1983).
[23] R. Griffiths, Nucl. Instrum. Methods **91**, 377 (1971).
[24] A. Notea, Nucl. Instrum. Methods **91**, 513 (1971).
[25] D.F. Crisler, J.J. Jarmer, and H.B. Eldridge, Nucl. Instrum. Methods **94**, 285 (1971).
[26] G.J. McCallum and G.E. Coote, Nucl. Instrum. Methods **130**, 189 (1975).
[27] R.J. Gehrke, R.G. Helmer, and R.C. Greenwood, Nucl. Instrum. Methods **147**, 405 (1977).
[28] K. Debertin and U. Schötzig, Nucl. Instrum. Methods **158**, 471 (1979).
[29] U. Schötzig, K. Debertin, and K.F. Walz, Nucl. Instrum. Methods **169**, 43 (1980).
[30] Y. S. Lee, T. Hukutome, M. Kobayashi, T. Horiguchi, and H. Inoue, J. Sci. Hiroshima University A **59**, 1 (1995).
[31] B. Souček, Nucl. Instrum. Methods **28**, 306 (1964).
[32] H.H. Bolotin, M.G. Strauss, and D.A. Mcclure, Nucl. Instrum. Methods **83**, 1 (1970).
[33] M. Wiernik, Nucl. Instrum. Methods **96**, 325 (1971); **95**, 13 (1971).
[34] G. Azuelos, J.E. Crawford, and J.E. Kitching, Nucl. Instrum. Methods **117**, 233 (1974).
[35] E.J. Cohen, Nucl. Instrum. Methods **121**, 25 (1974).
[36] S.N. Fedotov and N.G. Volkov, Nucl. Instrum. Methods **122**, 463 (1974).
[37] K. Debertin and U. Schötzig, Nucl. Instrum. Methods **140**, 337 (1977).
[38] A.H. Wapstra and G. Audi, Nucl. Phys. **A432**, 1 (1985).
[39] A. Bisi, E. Germagnoli, L. Zappa, and E. Zimmer, Nuovo Cimento **2**, 290 (1955).